Archives available at journals.mriindia.com

International Journal of Advanced Electrical and Electronics Engineering

ISSN: 2278-8948

Volume 12 Issue 01, 2023

Power-Quality Enhancement in A PV-FED D-STATCOM with LUO-Converter Interface and IoT Parameter Monitoring

[1]Akshaya A, [2]Ragesh R, [3]Saju S, [4]Sunil S, [5]Shajini Sheebha M E

[1,2,3,4,5]Department of Electrical and Electronics Engineering, Stella Mary's College of Engineering, Aruthenganvilai, Kanyakumari District, Tamil Nadu 629202, India

Peer Review Information

Submission: 13 Jan 2023
Revision: 16 Feb 2023
Acceptance: 09 March 2023

Keywords

D-STATCOM, Power Quality, Photovoltaic System, Luo Converter, Maximum Power Point Tracking, Reactive Power Compensation, Total Harmonic Distortion, IoT Monitoring, ESP8266.

Abstract

This paper reports the design and hardware realisation of a photovoltaic-fed distribution static compensator intended to improve voltage stability and reduce harmonic distortion at the point of common coupling, with an ESP8266-based node publishing photovoltaic parameters for remote monitoring. The conversion chain, comprising array, positive-output re-lift Luo converter, DC link, voltage-source inverter and shunt coupling, is formalised together with the compensation, tracking and reference-generation relations. The paper then distinguishes carefully between three categories that the source material does not separate. The photovoltaic stage, Luo converter, inverter, shunt branch, and monitoring display were built, while neuro-fuzzy MPPT and recurrent-neural-network reference generation remain design intentions rather than experimentally realised controller blocks themselves. Critically, no electrical quantity was logged at any node: no source-current spectrum, total harmonic distortion, power factor, DC-link transient, array power or tracking-efficiency measurement exists, so the compensation performance the device is built to deliver cannot be evaluated and no value is reported. The voltages of 394 V and 406 V appearing in the record are shown to belong to a cited baseline study of a different topology, not to this prototype, and are relabelled accordingly. This revision adds three elements. The distortion limits the compensator would have to meet are stated from IEEE Std 519-2022 rather than left implicit. The advantage claimed for the re-lift topology is made quantitative: for a tenfold voltage gain the re-lift stage requires a duty ratio of 0.80 against 0.90 for a simple boost, which is the difference between operating inside and outside the region where conduction and reverse-recovery losses dominate. And two reference entries that named no publication are replaced with identifiable sources, one of which establishes the night-time compensation capability the paper proposes to test. A staged measurement plan is specified which separates the converter, the compensator and the tracking algorithm so that any future improvement can be attributed to the block responsible.

Nomenclature

Symbol	Meaning
v_{pcc}, i_s	Point-of-common-coupling voltage (V) and source current (A)
i_L, i_c	Load current and compensating current injected by the shunt branch (A)

V_{dc}, C_{dc}	DC-link voltage (V) and capacitance (F)
V_{pv}, I_{pv}, P_{pv}	Array voltage (V), current (A) and power (W)
P_{mpp}	Power available at the array maximum power point (W)
D, G	Converter duty ratio and voltage gain V_o/V_{in}
V_{in}, V_o, I_o	Converter input and output voltage (V) and output current (A)
Q, X_c	Reactive power exchanged at the PCC (VAr) and coupling reactance (Ω)
V_{inv}, δ	Inverter output voltage (V) and its angle relative to the PCC
THD, PF	Total harmonic distortion (%) and power factor
η_{mppt}	Tracking efficiency (%)
Δi, f_s	Hysteresis band (A) and switching frequency (Hz)
L_1, L_2, C	Luo converter inductances (H) and capacitance (F)

Introduction

Distribution networks increasingly host both nonlinear loads, which inject harmonic current, and inverter-interfaced generation, whose output varies with the resource. Both stress voltage quality at the point of common coupling, and the distribution static compensator has become the standard shunt-connected remedy: by injecting a controlled current it can correct power factor, support voltage and cancel load harmonics [1], [2].

Coupling a photovoltaic array to such a compensator is attractive because the inverter and DC link already exist; the array then supplies real power through the same hardware that provides compensation [6]. Doing so requires a DC-DC stage that both boosts the array voltage to a usable DC-link level and presents the array with its maximum power point. This paper reports such a system, built around a positive-output re-lift Luo converter and augmented with an ESP8266 node that publishes array parameters for remote monitoring.

The paper documents the design in full and is explicit about a distinction the project record blurs: which parts of the described architecture exist in the constructed hardware, which are design intent, and which performance claims the campaign can support.

1. Problem Statement

Reports of photovoltaic-fed compensators routinely combine an advanced control proposal, whether neuro-fuzzy tracking or recurrent-network reference generation, with a photograph of a working prototype and a set of performance figures, without making clear which figures came from which artefact. The gap addressed here is that separation, together with the observation that a compensator's central claim, being harmonic reduction, is unverifiable without a current spectrum however sophisticated the control description.

2. Objectives

The specific objectives of the work are as follows:

- To consolidate the model of the photovoltaic-fed compensator chain: array, re-lift Luo converter, DC link, inverter and shunt coupling.
- To classify the design explicitly into elements that were built, elements described only, and quantities that were not measured.
- To trace the provenance of every numeric value appearing in the record, and to exclude from the results any figure belonging to a cited study.
- To state the distortion limits such a compensator would have to meet, in the units the governing standard uses.
- To quantify the advantage claimed for the re-lift topology rather than asserting it.
- To specify a staged measurement plan that attributes performance to the converter, the compensator or the tracker rather than to the system as a whole.

3. Scope and Delimitation

The study covers the modelling, the hardware realisation and the specification of the measurements that were absent. It excludes any claim of total harmonic distortion, power factor, reactive compensation, tracking efficiency, DC-link regulation quality or converter efficiency for this build, because none was measured. It excludes the neuro-fuzzy tracker and the recurrent-network reference generator, because neither is evidenced in the constructed controller. And it excludes the 394 V and 406 V figures found in the record, for the reason given in Section V-D.

4. Contributions

1. A consolidated model of the photovoltaic-fed compensator chain: array, re-lift Luo converter, DC link, inverter and shunt coupling.

2. An explicit three-way classification of the design into built, described-only and unmeasured elements.
3. Correction of the record: the 394 V and 406 V figures are identified as belonging to a cited baseline of a different topology, not to this prototype.
4. A statement of the applicable distortion limits from IEEE Std 519-2022, new to this revision, so that a future result has a criterion to be judged against.
5. A quantitative evaluation of the re-lift topology's duty-ratio advantage, new to this revision, which converts a qualitative design argument into a computed one.
6. Replacement of two reference entries that named no publication with identifiable sources, one of which establishes the night-time compensation capability the paper proposes to test.
7. A staged measurement plan that attributes performance to the converter, the compensator or the tracker rather than to the system as a whole.

The remainder of the paper is organised as follows. Section II reviews related work and fixes the applicable limits. Section III develops the relations. Section IV describes the prototype. Section V reports the results and their honest reading. Section VI discusses the findings, Section VII states the limitations, and Section VIII gives the assessment framework. Sections IX and X give the conclusion and the future scope.

Related Work

Ghosh and Ledwich [1] give the standard treatment of custom power devices and the shunt-compensator control laws that the distribution static compensator implements. Singh and colleagues [2] survey active-filter control and establish the hysteresis-band trade-off between tracking accuracy, switching frequency and residual ripple used in Eq. (8).

On the converter stage, Luo [3] developed the voltage-lift and re-lift converter family whose positive-output topology is adopted here, showing that the lift technique raises voltage gain without the extreme duty ratios a simple boost stage would demand; Section V-E makes that comparison numerical. For maximum power point tracking, Esram and Chapman [4] compare tracking algorithms and define the tracking efficiency of Eq. (4). Neuro-fuzzy trackers of the adaptive network-based fuzzy inference type are reported to improve convergence under rapid irradiance change at the cost of training and complexity; the general comparison against conventional baselines is given in [4], and the specific claim is treated in this paper as design intent rather than established fact, for the reason set out in Section V-B.

On photovoltaic-integrated compensation, Varma and colleagues established that a photovoltaic inverter can be operated as a static compensator, first for night-time voltage regulation when the array produces nothing [5], and subsequently as a full smart-inverter control in which the entire inverter capacity is released for compensation at night and, during a daytime disturbance, real power generation is briefly suspended so that the whole rating becomes available [6]. This is an argument for the topology that is independent of generation, and it is the basis of the night-time test proposed in Section VIII. The ESP8266 platform [7] provides the monitoring layer.

Table 1. Representative Related Work and its Relation to This Study

Ref.	Year	Focus and scope	Method and validation	Relation to this work
[1]	2002	Custom power devices	Control design; simulation	Compensator structure and laws
[2]	1999	Active filter control review	Survey	Hysteresis control trade-offs
[3]	1999	Voltage-lift and re-lift converters	Analysis; experiment	The Luo stage used here
[4]	2007	MPPT algorithm comparison	Review; simulation	Defines tracking efficiency; conventional baselines
[5]	2009	Night-time PV solar farm as STATCOM	Analysis; simulation	Establishes night-time reactive support
[6]	2018	PV-STATCOM smart inverter for distribution	Analysis; field demonstration	Motivates PV-fed compensation on a 24-hour basis
[7]	—	ESP8266 platform	Vendor documentation	Monitoring and Wi-Fi stage
[8]	2022	IEEE Std 519 harmonic control	Recommended practice	The limits a result must be compared against

Two entries have been corrected in this revision. An earlier draft carried a citation for neuro-fuzzy tracking that named no publication, referring the reader instead to the tracking comparison in another reference; it has been removed and the argument is now attributed in the text rather than to an unverifiable source. A second entry described photovoltaic-inverter compensation as an author name followed by related literature; it has been replaced by the two specific papers now at [5] and [6].

1. The Limits a Result Would Have to Meet

The central claim such a device invites is a reduction in harmonic distortion at the point of common coupling. That claim is meaningful only against a stated limit, and the governing document is IEEE Std 519, of which the 2022 edition is current. Table 2 states the applicable values, and Fig. 1 shows the current limits.

Table 2. Distortion Limits from IEEE Std 519-2022

Quantity	Limit	Applicability
Voltage, individual harmonic	5.0 %	Systems at or below 1.0 kV, at the point of common coupling
Voltage, total harmonic distortion	8.0 %	Systems at or below 1.0 kV
Voltage, total harmonic distortion	5.0 %	Systems above 1.0 kV and up to 69 kV
Current, 3 ≤ h < 11	4.0 % of I_L	Short-circuit to demand-current ratio below 20
Current, 11 ≤ h < 17	2.0 % of I_L	Short-circuit to demand-current ratio below 20
Current, 17 ≤ h < 23	1.5 % of I_L	Short-circuit to demand-current ratio below 20
Current, 23 ≤ h < 35	0.6 % of I_L	Short-circuit to demand-current ratio below 20
Current, 35 ≤ h ≤ 50	0.3 % of I_L	Short-circuit to demand-current ratio below 20
Current, total demand distortion	5.0 %	Short-circuit to demand-current ratio below 20

Values are the limits published in IEEE Std 519-2022 [8]. Even harmonics of order six and below are limited to half the tabulated values. Note that the standard limits total demand distortion, referred to the maximum demand load current, whereas Eq. (2) defines total harmonic distortion, referred to the fundamental actually flowing; the two coincide only at rated demand, so a reported figure must state which measure it is and under what load. Nothing in this table was measured on the prototype described in Section IV.

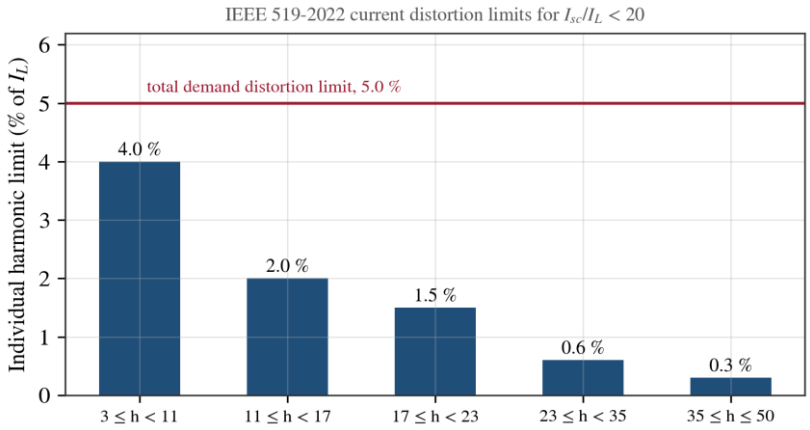

Figure 1: Current distortion limits from IEEE Std 519-2022 for a short-circuit to demand-current ratio below 20.

System Modelling

1. Compensation at the Point of Common Coupling

With the shunt branch injecting a compensating current, the source current is

$$i_s = i_L - i_c \tag{1}$$

so choosing the injected current equal to the harmonic and reactive components of the load

current leaves a sinusoidal, in-phase source current. The residual quality is measured by

$$THD = \frac{\sqrt{\sum_{h\geq 2} I_{s,h}^2}}{I_{s,1}} \times 100\%, \qquad PF = \frac{P}{S} \tag{2}$$

and the reactive exchange available from the compensator is bounded by the inverter rating and DC-link voltage,

$$Q = \frac{V_{pcc}(V_{inv}\cos\delta - V_{pcc})}{X_c} \tag{3}$$

Equations (2) and (3) are the quantities the device exists to deliver; Section V-C explains why neither can be evaluated here.

2. Array and Tracking

The array operating point is set by the converter duty ratio. Tracking efficiency over an interval is

$$\eta_{mppt} = \frac{\int P_{pv}(t)\,dt}{\int P_{mpp}(t)\,dt} \times 100\% \tag{4}$$

which requires simultaneous logging of array voltage, array current and the true maximum available power, illustrated in Fig. 2. None of these was recorded.

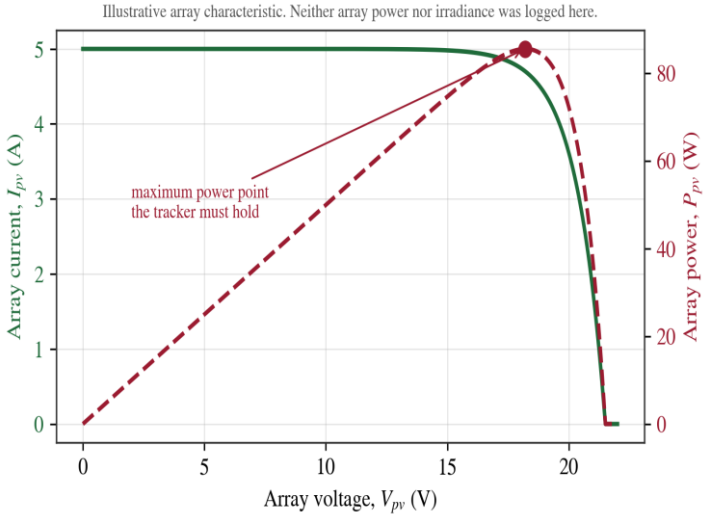

Figure 2: Illustrative array characteristic showing the operating point a tracker must hold. Neither array power nor irradiance was logged here.

3. Positive-Output Re-Lift Luo Converter

The re-lift topology uses two inductors and a lift capacitor network to obtain a high positive-output gain. For the positive-output re-lift stage in continuous conduction, the ideal voltage transfer ratio is

$$\frac{V_o}{V_{in}} = \frac{2}{1-D} \tag{5}$$

which for a given output voltage requires a markedly lower duty ratio than a single boost stage, keeping the switch away from the extreme duty region where conduction and reverse-recovery losses dominate. Section V-E quantifies that difference. Inductor and capacitor selection follows the ripple constraints

$$L \geq \frac{V_{in} D}{f_s \,\Delta I_L}, \qquad C \geq \frac{I_o D}{f_s \,\Delta V_o} \tag{6}$$

The record does not state the inductances, the capacitance, the switching frequency or the design ripple, so Eqs. (5) and (6) are given as the governing relations rather than evaluated for this build.

4. Reference Generation and Gating

The compensating reference is obtained from the load current by extracting its fundamental active component and subtracting,

$$i^{*} = i_L - \bar{i}_1 \sin(\omega t + \phi_1) \tag{7}$$

and gating is produced by a hysteresis comparator,

$$S = 1 \;\; (i_c < i^{*} - \Delta i/2); \qquad S = 0 \;\; (i_c > i^{*} + \Delta i/2) \tag{8}$$

with the DC link regulated so that the inverter draws the real power it needs,

$$C_{dc} V_{dc} \frac{dV_{dc}}{dt} = P_{pv} + P_{grid} - P_{inv,loss} \tag{9}$$

Prototype

1. Architecture

Fig. 3 shows the system. The array feeds the Luo converter, whose output supports the DC link of a voltage-source inverter; the inverter is coupled to the point of common coupling through the shunt branch and supplies the load alongside the grid. An ESP8266 node samples array-side parameters and publishes them over Wi-Fi for remote display. The two items shown as absent at the foot of the figure are the ones on which the whole of Section V turns.

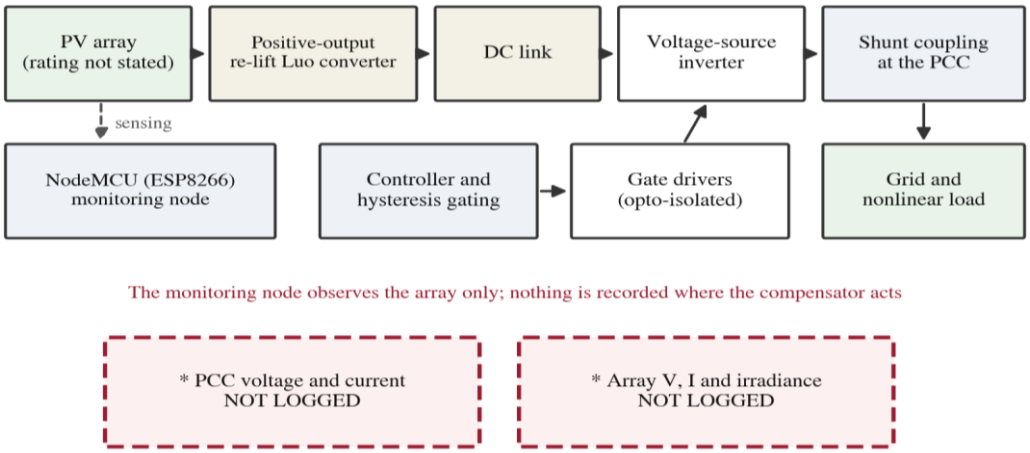

Figure 3: Prototype architecture. Sensing exists on the array side for display only; no logging path was provided at the point of common coupling.

2. Apparatus

Table 3 lists the prototype as documented.

Table 3. Prototype as Documented

Item	Type / rating	Quantity
PV array	Rating not stated in the record	1
DC-DC stage	Positive-output re-lift Luo converter	1
Inverter	Voltage-source, MOSFET bridge	1
Gate driver	Opto-isolated	4 or more
Monitoring node	NodeMCU (ESP8266)	1
Auxiliary supply	Bridge and regulator, 5 V and 15 V	1
Display	Remote, over Wi-Fi	1

The array rating, the converter inductances and capacitance, the switching frequency, the DC-link voltage and the coupling reactance are all absent from the record, so Eqs. (3), (5), (6) and (9) cannot be evaluated for this build even in principle.

Results

1. What the Campaign Established

The hardware was constructed and energised, and the monitoring node was shown publishing photovoltaic parameters to a remote display. Those two facts are the observed result, and they are reported without extension.

2. Built, Described and Unmeasured

The design text describes a neuro-fuzzy maximum power point tracker and a recurrent-neural-network reference generator. Neither appears in the constructed controller as documented, and no training data, network structure, membership functions or embedded implementation is recorded. They are therefore reported here as design intent, not as realised blocks, as Fig. 4 sets out. This distinction matters because both are load-bearing in the design's performance argument: the claimed tracking accuracy rests on the former and the claimed harmonic elimination on the latter.

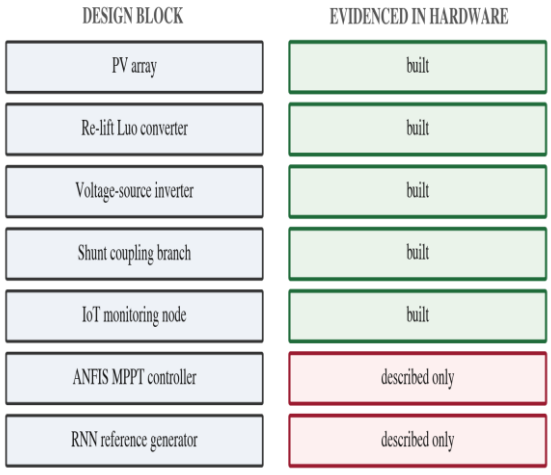

Figure 4: Design blocks classified by whether they are evidenced in the constructed hardware.

3. Why No Compensation Performance Is Reported

Evaluating a compensator requires measurements at the point of common coupling. The campaign recorded none:

- No source-current waveform or spectrum, so the distortion of Eq. (2) is unknown both before and after compensation;
- No voltage and current phase relationship, so power factor is unknown;
- No reactive exchange record, so Eq. (3) is unevaluated;
- No array voltage and current log or irradiance reference, so the tracking efficiency of Eq. (4) is unknown;
- No DC-link transient, so the regulation quality implied by Eq. (9) is unknown.

Accordingly, no distortion, power factor, efficiency or tracking figure appears in this paper, and none is estimated.

4. Provenance of the 394 V and 406 V Figures

The project record contains the statement that a controller mitigated sag and swell, bringing the system to 394 V and 406 V respectively. Read in context, those values belong to the review of prior work on a distributed power flow controller with a proportional-integral regulator, which is a different topology from the compensator built here, and describe that cited study's results rather than this prototype's. They are reproduced in Fig. 5 with that provenance stated, and they are excluded from every claim about the present system. Carrying such figures forward as one's own results is the specific failure this paper is written to avoid.

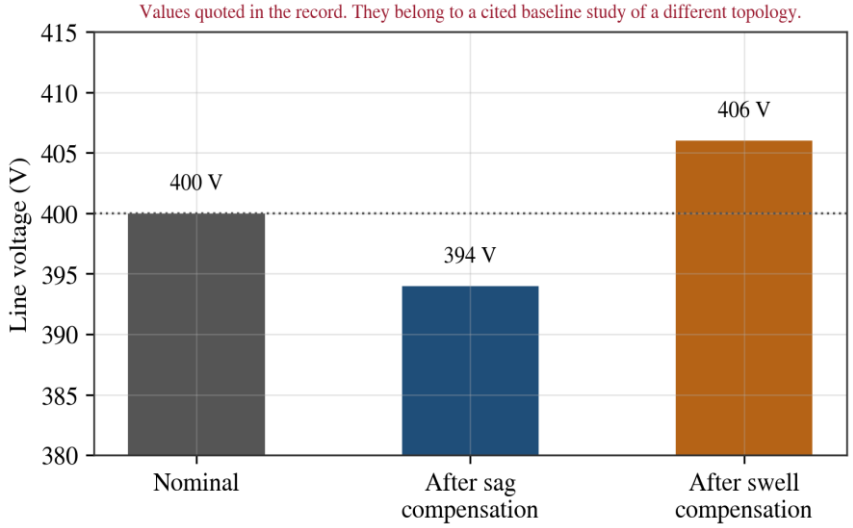

Figure 5: Sag and swell values quoted in the record. These belong to a cited baseline study of a different topology and are not results of this prototype.

5. Quantifying the Re-Lift Advantage

The converter choice is the one design decision in this work that can be evaluated without any measurement, because it follows from Eq. (5) alone. Inverting that relation and the corresponding boost expression gives the duty ratio each topology needs for a required gain,

$$D_{boost} = 1 - \frac{1}{G}, \qquad D_{re\text{-}lift} = 1 - \frac{2}{G} \tag{10}$$

Table 4 evaluates both, together with the triple-lift member of the same family, and Fig. 6 plots them.

Table 4. Duty Ratio Required for a Given Voltage Gain (Computed from Eqs. (5) and (10))

Required gain G	Boost or self-lift	Re-lift (used here)	Triple-lift
4	0.750	0.500	0.250
6	0.833	0.667	0.500
8	0.875	0.750	0.625
10	0.900	0.800	0.700
15	0.933	0.867	0.800
20	0.950	0.900	0.850

Computed from the ideal continuous-conduction transfer ratios. These are topology properties, not measurements of this converter, whose inductances, capacitance and switching frequency are undocumented. Real duty ratios are higher than the ideal values because of conduction and switching losses, which the ideal relations neglect.

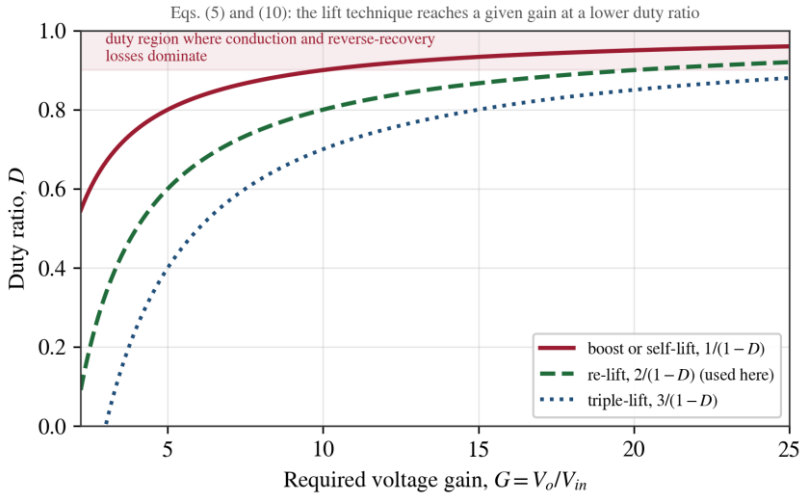

Figure 6: Duty ratio required against voltage gain for three members of the lift family, from Eqs. (5) and (10).

The result gives the design argument its force. For a tenfold gain, which is representative of stepping a low-voltage array up to a usable DC-link level, a boost stage must run at a duty ratio of 0.90 while the re-lift stage reaches the same gain at 0.80. That is the difference between an off-time of 10 % and 20 % of the switching period, and it is precisely in the region above about 0.9 that conduction and reverse-recovery losses begin to dominate and that regulation becomes difficult. The topology choice is therefore justified, and this is the one claim in the paper that stands without instrumentation. It is worth noting explicitly that it is a claim about the topology and not about this converter, whose realised gain, ripple and efficiency remain unmeasured.

6. The Monitoring Stage on Its Own Terms

The monitoring node worked, and remote visibility of array parameters is a genuine convenience. Its limits should be stated: the published values are uncalibrated sensor readings, no time-stamped history was retained, and the node observes the array only. It sees nothing at the point of common coupling, which is where the compensator's effect appears. A monitoring stage that cannot observe the quantity the project aims to improve adds operational convenience but no evaluative power.

7. What the Campaign Supports

Table 5 states the position element by element.

Table 5. Built, Described and Indeterminate Elements

Quantity or capability	Value	Status
Hardware constructed	yes	demonstrated
IoT parameter display	functions	demonstrated
PV, Luo, inverter and shunt stages	present	built
Neuro-fuzzy MPPT controller	—	described only; not evidenced in hardware
Recurrent-network reference generator	—	described only; not evidenced in hardware
Source-current spectrum	—	not recorded
Total harmonic distortion, before and after	—	indeterminate
Power factor at the PCC	—	indeterminate
Reactive compensation Q	—	not measured
Tracking efficiency η_{mppt}	—	not measured
DC-link transient	—	not recorded
Converter L, C and switching frequency	—	not documented
Array rating and DC-link voltage	—	not documented

394 V and 406 V figures	see Section V-D	cited baseline of a different topology
Duty-ratio advantage of the re-lift stage	0.80 against 0.90 at G = 10	computed, Eqs. (5) and (10)
Applicable current distortion limit	5.0 % total demand distortion	standard [8], not a measurement

Discussion

The design side of this work is coherent and the topology choice is well made. The measurement side is empty, and the two intelligent blocks that carry the design's performance argument are absent from the hardware. Stating this plainly is more useful than presenting the system as complete, because it identifies exactly what a second iteration would have to add.

1. The Order in Which the Gaps Should Be Closed

There is a natural priority among them. A single two-channel record at the point of common coupling would convert a construction report into a compensation result, and costs nothing beyond the oscilloscope already available during the build. Array instrumentation comes next, since it makes the tracking claim testable. The intelligent blocks come last, because implementing a neuro-fuzzy tracker before there is any means of measuring tracking efficiency would produce a controller whose advantage could not be demonstrated even if it existed.

2. Qualitative Position

Table 6 sets out the structural properties that can be asserted, each with the relation or source that supports it.

Table 6. Qualitative Properties and Their Basis

Feature	Property	Basis
Shunt compensation	Corrects power factor; cancels load harmonics	[1], Eqs. (1), (2)
Re-lift Luo stage	Reaches a given gain at a lower duty ratio	Eqs. (5), (10), Table IV
PV-fed DC link	Shares the inverter between generation and compensation	[5], [6]
Night-time operation	Full inverter rating available when the array is idle	[5], [6]
Hysteresis gating	Simple; variable switching frequency set by the band	Eq. (8)
Neuro-fuzzy tracking	Faster convergence claimed; needs measurement	[4], Section V-B
IoT node	Remote visibility of the array only	Section V-F
Distortion reporting	Meaningless without load condition and reference current	Eq. (2), [8]

Limitations

The following limitations bound every claim made in this paper.

- No electrical quantity was logged at any node. Distortion, power factor, reactive exchange, tracking efficiency, DC-link regulation and converter efficiency are indeterminate for this build, not merely uncertain, and none is estimated.
- The neuro-fuzzy tracker and the recurrent-network reference generator are not evidenced in the constructed controller. Every performance claim resting on them is therefore design intent.
- The array rating, converter inductances and capacitance, switching frequency, DC-link voltage and coupling reactance are undocumented, so the design cannot be reproduced from this paper.
- The duty-ratio figures of Table IV are ideal continuous-conduction values for the topologies named. They are properties of the topology, not measurements of this converter, and real duty ratios are higher because losses are neglected.
- The distortion limits of Table II are published criteria, not measurements, and they bound total demand distortion rather than the total harmonic distortion of Eq. (2). The two differ except at rated demand.
- The 394 V and 406 V figures belong to a cited study of a different topology and are excluded from all claims about this prototype.

- The monitoring node publishes uncalibrated array-side readings with no retained time-stamped history, and observes nothing at the point of common coupling.
- No night-time compensation test was performed, so the capability established in the literature for this topology class is not demonstrated for this build.

Proposed Assessment Framework

Fig. 7 shows the staged plan. Each stage isolates one block so that a measured change can be attributed to it.

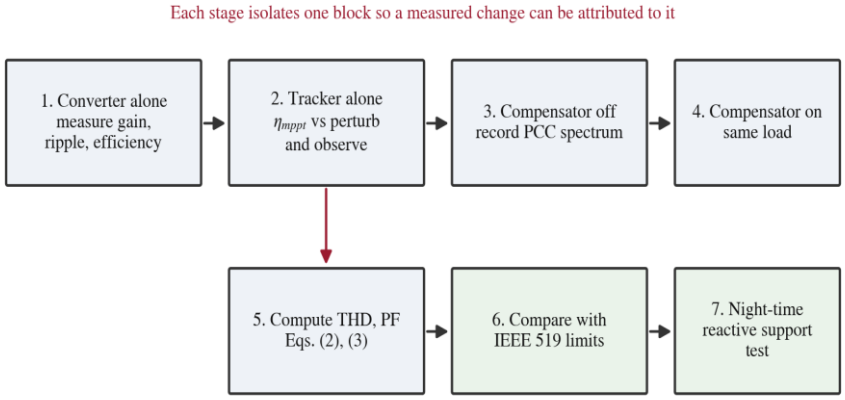

Figure 7: Staged assessment isolating converter, tracker and compensator, ending with the night-time reactive support test.

1. Minimum Instrumentation

A single two-channel record of point-of-common-coupling voltage and source current, taken with the compensator disabled and then enabled under an unchanged load, converts this work from a construction report into a compensation result. That measurement requires no hardware the laboratory does not already possess, since an oscilloscope was available during the build. Recording the maximum demand current at the same time allows the result to be compared against Table II.

2. Evaluating the Intelligent Blocks

If the neuro-fuzzy tracker and the recurrent-network reference generator are implemented in a future revision, each should be compared against a conventional baseline, being perturb-and-observe and a fixed synchronous-frame extractor respectively, on identical hardware and load. Only a paired comparison of that kind supports a claim that the intelligent method is responsible for an improvement.

3. Measurement Plan

Table 7 sets out the measurements required, and Table VIII gives the context values that are cited figures or literature rather than results.

Table 7. Measurement Plan Required to Make the Assessment Quantitative

Measurement	Method	What it yields
Measure at the PCC	Voltage and source current with the compensator disabled and enabled	Distortion and power factor through Eq. (2)
Record the demand current	Maximum demand load current over the window	Allows comparison against the limits of Table II
Reactive exchange	Phase-resolved voltage and current at the coupling point	Q through Eq. (3)
Instrument the array	Log V_{pv} and I_{pv} with an irradiance reference	Tracking efficiency through Eq. (4)
Document the converter design	Record L_1, L_2, C, switching frequency and design ripple	Allows Eqs. (5) and (6) to be checked against measurement
DC-link transient	Repeatable load step with V_{dc} logged	Regulation quality implied by Eq. (9)
Paired algorithm comparison	Intelligent block against a conventional baseline, all else fixed	Attributes any improvement to the algorithm
Night-time reactive support	Operate with zero array output and measure Q at the PCC	Verifies the distinctive capability of the topology [5], [6]

Table 8. Illustrative and Cited Figures (Not Results of This Work)

Item	Value	Status
Sag and swell compensation	394 V and 406 V	cited baseline of a different topology, Section V-D
Current total demand distortion limit	5.0 %	standard [8]
Duty ratio at G = 10, re-lift against boost	0.80 against 0.90	computed, Eqs. (5) and (10)

Entries are cited figures, published limits or values computed from stated relations. None was measured in this work. An earlier draft of this table also carried general photovoltaic cell and module efficiency ranges which had no bearing on any claim in the paper and which were, in the case of the module figure, well below current commercial values; they have been removed rather than updated, since the paper makes no argument that depends on them.

Conclusion

A photovoltaic-fed distribution static compensator with a positive-output re-lift Luo converter interface and an ESP8266-based parameter monitor was designed and built. The compensation, tracking, converter-gain and DC-link relations were consolidated, and the hardware was energised with the monitoring node shown publishing array parameters remotely.

The paper then separated what the campaign supports from what it does not. The array, converter, inverter, shunt branch and monitoring node exist in the build; the neuro-fuzzy maximum power point tracker and the recurrent-neural-network reference generator are described in the design but are not evidenced in the constructed controller and are reported as design intent. No electrical measurement was recorded at any node, so total harmonic distortion, power factor, reactive compensation, tracking efficiency and DC-link regulation are all indeterminate and none is estimated. The 394 V and 406 V values in the record were traced to a cited baseline study of a different topology and excluded from all claims about this prototype.

This revision added the criteria and the one computable design result. IEEE Std 519-2022 limits current total demand distortion to 5.0 % for a short-circuit to demand-current ratio below 20, with individual harmonic limits from 4.0 % down to 0.3 % by order, and it limits total demand distortion rather than the total harmonic distortion of Eq. (2), so a future figure must state which measure it is and under what load. The advantage claimed for the re-lift topology was made quantitative: at a tenfold voltage gain the re-lift stage operates at a duty ratio of 0.80 where a boost stage needs 0.90, which places the switch outside rather than inside the region where conduction and reverse-recovery losses dominate. This is the one claim in the paper that stands without instrumentation, and it is a property of the topology rather than a measurement of this converter.

A staged assessment plan was specified, being converter, then tracker, then compensator, ending with the night-time reactive support test that the literature establishes as a distinctive capability of this topology class. A single two-channel measurement at the point of common coupling, using equipment already available during the build, would convert this construction report into a compensation result.

Future Work

Several extensions follow directly from the limitations above.

- Measure at the point of common coupling-Record voltage and source current with the compensator disabled and enabled, compute Eq. (2) from both, and log the demand current so the result can be checked against Table 2.
- Instrument the array-Log array voltage and current with an irradiance reference so that Eq. (4) becomes evaluable.
- Document the converter design-Record the inductances, capacitance, switching frequency and design ripple so that Eqs. (5) and (6) can be checked against measurement, and so that the computed duty-ratio advantage of Table IV can be confirmed on the actual hardware.
- Implement or withdraw the intelligent blocks-Either embed and evaluate the neuro-fuzzy tracker and the recurrent-network extractor against conventional baselines, or state that the realised system uses conventional control.
- Extend monitoring to the point of common coupling-Publish compensation-side quantities, so that the monitoring stage can observe what the project sets out to improve.
- Test night-time compensation-Verify reactive support with zero array output, which the literature establishes as a distinctive capability of this topology

and which this build has not demonstrated.

Acknowledgment
The authors thank the Department of Electrical and Electronics Engineering, Stella Mary's College of Engineering, for laboratory facilities and guidance during the project.

References

A. Ghosh and G. Ledwich, Power Quality Enhancement Using Custom Power Devices. Boston: Kluwer Academic, 2002.

B. Singh, K. Al-Haddad, and A. Chandra, "A review of active filters for power quality improvement," IEEE Transactions on Industrial Electronics, vol. 46, no. 5, pp. 960-971, 1999.

F. L. Luo, "Positive output Luo converters: Voltage lift technique," IEE Proceedings - Electric Power Applications, vol. 146, no. 4, pp. 415-432, 1999.

T. Esram and P. L. Chapman, "Comparison of photovoltaic array maximum power point tracking techniques," IEEE Transactions on Energy Conversion, vol. 22, no. 2, pp. 439-449, 2007.

R. K. Varma, V. Khadkikar, and R. Seethapathy, "Nighttime application of PV solar farm as STATCOM to regulate grid voltage," IEEE Transactions on Energy Conversion, vol. 24, no. 4, pp. 983-985, 2009.

R. K. Varma and E. M. Siavashi, "PV-STATCOM: A new smart inverter for voltage control in distribution systems," IEEE Transactions on Sustainable Energy, vol. 9, no. 4, pp. 1681-1691, October 2018.

Espressif Systems, "ESP8266EX datasheet," vendor documentation.

IEEE Std 519-2022, "IEEE Standard for Harmonic Control in Electric Power Systems," superseding IEEE Std 519-2014.